RESEARCH PAPER

Synthesis and Performance Evaluation of Ti-Doped CaCO3 Nanocomposites for Environmental and Biomedical Applications

T. Sathishpriya[1], E. Thenpandiyan[2*], D. Mohanambal[3], Yengkokpam Robinson Singh[4], N. Prathap[5], A. Ajith[6]

[1]Loyola Institute of Technology, Department of Physics, Palanchur, Chennai – 600 123, Tamil Nadu, India
[2*]Department of Physics, Academy of Maritime Education and Training, Kanathur, Chennai - 603 112, Tamil Nadu, India
[3]Loyola Institute of Technology, Department of Chemistry, Palanchur, Chennai – 600 123, Tamil Nadu, India
[4]Department of Physics, Kamakhya Pemton College, Hiyangthang, Imphal West, Manipur – 795 009, India
[5]Department of Environmental Science, Periyar University, Salem – 636 011, Tamil Nadu, India
[6]Department of Physics, Dr. Mahalingam College of Engineering and Technology, Pollachi – 642 003, Tamil Nadu, India

***Corresponding author: E. Thenpandiyan, Department of Physics, Academy of Maritime Education and Training, Kanathur, Chennai - 603 112, Tamil Nadu, India**
Email: esthenpandiyan2@gmail.com

Received: 25th May, 2026; **Revised:** 6th June, 2026; **Accepted:** 8th June, 2026; **Available Online:** 09th June, 2026

ABSTRACT

A novel technique of biomimetic method has been used for the synthesis of Ti-doped calcium carbonate nanocomposites (TC) for photocatalytic and antibacterial activities. The prepared various concentrations (0.02, 0.04, 0.06, 0.08, and 0.1 M) of TC, Ti-doped calcium carbonate nanocomposites, were subjected to the different spectroscopic techniques. The absorption and emission properties were analyzed through UV-DRS and PL analysis. From the results, 0.06 M of TC exhibits higher absorption (268 nm) and emission values (465), and 0.1 M of TC shows lower absorption (260 nm) and emission (457 nm) values when compared with other concentrations. The functional and structural analyses of the products were characterized via FTIR and XRD analysis. From this, the successful incorporation of titanium in the $CaCO_3$ host was confirmed by the presence of metal oxide peaks in the range of around 450 cm^{-1}. The rhombohedral structure of $CaCO_3$ was confirmed through XRD analysis, and the calculated crystallite size was in the range of 25-35 nm, respectively. The spherical morphology of the prepared TC was obtained through FE-SEM analysis. From the EDX and mapping, it shows the confirmation of dopant ions (Ti^{2+}/Ti^{4+}) in the $CaCO_3$ host. The optimized samples were subjected to the photocatalytic and antibacterial activities. From the photocatalytic activity, 0.06 M of TC exhibits good degradation efficiency (95%) against malachite green dye during 110 min under UV irradiation. The antibacterial performance of 0.1 M of TC against different bacteria such as S. aureus, S. pyogenes, K. pneumoniae, and E. coli was analyzed. From the results, it shows a higher zone of inhibition for both gram-positive and gram-negative bacteria at a dose concentration of 1000 µg/ml. These results show that Ti-doped $CaCO_3$ nanocomposites are appropriate for biological applications and a promising sustained photocatalyst.

Keywords: Titanium; $CaCO_3$; malachite green dye; Antibacterial activity; Biomimetic method.

How to cite this article: Sathishpriya T, Thenpandiyan E, Mohanambal D, Singh YR, Prathap N, Ajith A. Synthesis and Performance Evaluation of Ti-Doped CaCO3 Nanocomposites for Environmental and Biomedical Applications. Int J Drug Deliv Technol. 2026;16(57s): 1797-1806. DOI: 10.25258/ijddt.16.57s.180

Source of support: Nil.

Conflict of interest: None.

1. Introduction

A number of water contaminants, mostly dyes, have been brought about by recent advancements and industrial development [1]. One of the biggest environmental issues is wastewater and the treatment of complex contaminants in wastewater. Furthermore, contemporary pollutants in wastewater include synthetic dyes. Because dye molecules are often complex, non-biodegradable, and environmentally stable, they are challenging to remove or break down [2]. Because dyes are highly stable and fragrant, physical and biological treatments typically fail to remove them from wastewater [3].

Microorganisms in water, for instance, are unable to break down colors and exhibit certain carcinogenic substances during the decomposition process. Furthermore, physical methods like reverse osmosis [4], ultrafiltration [5], and activated carbon adsorption [6] might move the organic chemical to a different phase, which may result in secondary contamination. Secondary pollutants cause solid waste management and necessitate a post-treatment procedure, which results in additional expenses [7, 8]. A photocatalysis degradation method that may remove contaminants from wastewater, particularly dyes, is one of the promising, straightforward, and economical solutions [9–12].

Photocatalytic degradation, a cheap and efficient technique for transforming pollutants, is

one of the intriguing wastewater treatment approaches [13–18]. Semiconducting materials must function as a photocatalyst for the photocatalytic degradation process, which can be triggered by absorbing irradiation photons of the right wavelength. The electrons in the valence band (VB) are energized and promoted to the conduction band (CB) when the photocatalyst absorbs the photon energy, leaving holes at VB [19].

The reported nanoparticles used to create nanocomposite hydrogels are typically costly or challenging to scale up. Finding inexpensive, scalable, and safe nanomaterials is necessary since nanocomposites have demonstrated significant promise in improving the dye absorption of hydrogels. $CaCO_3$ is a cheap, easily accessible mineral that may be found in rocks all around the world. Additionally, it can be synthesized and is present in animal membranes including those of snails and crabs as well as eggshells.Many different industries employ $CaCO_3$ as a filler [20,21]. $CaCO_3$ is frequently employed as an inexpensive adsorbent [22] in the removal of heavy metals [23], oil spills [24], and dyes from water [25]. $CaCO_3$ particles can be coated for better performance [26, 27] and have a large surface area [28, 27].

Research on the degradation of organic dyes using pure metallic nanoparticles is frequently conducted. By altering the electrical structure, doping, on the other hand, increases catalytic activity while introducing flaws into the native semiconductor's flawless crystal lattice. These kinds of defects can trap electrons or holes created during photoexcitation. Increasing the catalytic activation of strong bonds is another important function of defect sites, such as vacancy production, which helps the process kinetically [29]. Additionally, doping may cause an additional charge carrier to develop in the photocatalyst, which could cause the original bandgap to broaden or constrict. Doping can thereby change photocatalytic activity toward substrate, limit recombination trap sites, and adjust light absorption [29].

One of the most crucial minerals used in semiconductors is titanium dioxide (TiO_2) powder [30]. Because the band gap of nanoparticles increases with decreasing size and tiny TiO_2 particles provide a very large surface area, nanosizeTiO_2NPs have a number of distinctive features [31]. Because of its huge surface area, chemical and physical stability, corrosion resistance, non-toxicity, comparatively low cost, and stable colloidal suspension, TiO_2 nanostructures have a high sustainable efficiency. [32].Using a nonhydrolitic technique, Stoyanova et al. produced TiO_2/ZnO nanocomposites in powder form and investigated their bactericidal characteristics.

When exposed to UV light, the produced TiO_2/ZnO powders are very effective against E. coli [33]. Wang et al. synthesized TiO_2/ZnO nanomaterials at 500°C using the sol-gel method and examined their antibacterial activity when exposed to visible light. They discovered that C. albicans is more susceptible to the antibacterial effect than S. aureus and E. coli [34]. High-quality ZnO doped TiO_2 nanocrystals were produced chemically by
Kaviyarasu et al [35]. TiO_2 doped with ZnO has been demonstrated to be effective in antibacterial applications [35].

The photocatalytic dye degradation of zinc oxide and titanium oxide nanoparticles, both separately and in combination, is widely recognized. This study uses eggshell-derived calcium oxide (CaO) nanoparticles as a photocatalyst for efficient dye degradation, reusing kitchen waste (eggshell) in a sustainable way and at a lower cost than previously described materials.

This study presents a novel biomimetic synthesis approach for the fabrication of Ti-doped calcium carbonate nanocomposites (TC), which distinguishes it from conventional chemical or physical synthesis routes. By employing a biomimetic technique, titanium ions (Ti^{2+}/Ti^{4+}) can be carefully incorporated into the $CaCO_3$host lattice, improving its structural and functional characteristics.

The methodical study of different Ti doping concentrations (0.06 and 0.1 M) and their direct impact on optical, structural, photocatalytic, and antibacterial properties is a significant novelty.The optimized 0.06 M concentration is particularly useful as a sustainable photocatalyst since it shows excellent optical behavior and produces a high photocatalytic degradation efficiency (95%) of malachite green dye under UV irradiation. Furthermore, our work illustrates TC' dual-functional performance, which combines potent antibacterial qualities with effective photocatalytic activity.

Significant antibacterial efficiency against both Gram-positive and Gram-negative bacteria is demonstrated by the higher Ti concentration (0.1 M), suggesting that biological activity can be adjusted through doping levels. The successful creation of a multifunctional

nanocomposite is further highlighted by the demonstration of Ti incorporation into the $CaCO_3$ lattice, retention of rhombohedral structure, nanoscale crystallite size (25 and 35 nm), and spherical morphology.

2. Materials and techniques

2.1. Materials

Sucrose, anhydrous sodium carbonate, $TiCl_4$, Polymethyl methacrylate (PMMA), and hydrochloric acid (obtained from Sigma-Aldrich) were used in this investigation.

2.2 sample collecting

In Arisipalayam, Salem District, Tamil Nadu, India (latitude: 11◦65′ 92′ N; longitude: 78◦14′ 00"E), ten natural carbonate sources (dolomite rock), each weighing roughly 5 kg, were gathered. To eliminate organic waste and other contaminants, the obtained samples were subjected to a number of pretreatment procedures using diluted HCl.

2.3. Preparation of PMMA/$CaCO_3$:Ti

According to Venkidasamy et al. [36], PMMA/$CaCO_3$:Ti was prepared from dolomite rock ($CaMg(CO_3)_2$). A sample of crushed natural carbonate was ground into a fine powder using an agate mortar. The powder was sieved using a 90 µm stainless steel laboratory test sieve to get CaO.MgO. The resulting sample was then heated for two hours at 900 °C in a muffle furnace. 10 g of CaO.MgO powder was dissolved in 100 mL of a 1 mol sucrose solution to create nano $CaCO_3$. A 500 mL three-necked round-bottom flask was filled with the mixture after it was rapidly agitated for one hour at room temperature to produce a soluble calcium sucrose solution.

White precipitation resulted by adding a 1 mol solution of sodium carbonate (80 mL) dropwise over two hours at 80 °C to create nano calcium carbonate. After rinsing the precipitate more than three times with acetone and ultra-pure deionized water, the sample was filtered through Whatman filter paper and cooked to 60 °C in a hot air oven. The same method was used to create the Ti-doped PMMA/CaCO3 nanoparticles. Ten milliliters of PMMA, eighty milliliters of 1 mol sodium carbonate, and different concentrations of $TiCl_4$ (0.06 and 0.1 M) were added dropwise to the calcium sucrose solution.

The preparation of Ti-doped PMMA/$CaCO_3$ was demonstrated by the emergence of a white precipitate after the reaction was conducted at 80 °C for more than two hours. The precipitate was filtered using Whatman filter paper after being extensively cleaned several times with acetone and ultrapure deionized water to get rid of any remaining contaminants. Lastly, the sample was dried at 60 °C in a hot air oven [36].

2. 4 Characterization

UV-VIS-DRS spectra were obtained using an ISR-603 integrating sphere unit connected to a UV-VIS-NIR spectrometer with an operating range of 200–800 nm. The generated materials' photoluminescence spectra were examined using a Horiba JobinYvon Fluoromax-4 spectrofluorometer. An FTIR spectrometer (Make: SHIMADZU-8400 in transmittance mode; resolution ± 4 cm^{-1}; KBr pellet technique) was used to record the FTIR spectra. An X-ray diffractometer (X'pert PRO; CuKα radiation (λ=1.5406 Å), a 30 mA current, and an operating voltage of 40 kV. A Carl Zeiss Sigma 300 FESEM microscope (accelerating voltage range: 0.3 kV to 30 kV; resolution: 15 nm (1 kV) in high-vacuum mode
(HV)) was used for the product's morphological examination and elemental analysis.A Shimadzu-UV 1800 UV–Vis spectrophotometer (wavelength range: 200–800 nm) was used to record the optical absorption spectra of the materials.

2.5 In vitro antibacterial assay

The Disc diffusion method was used to evaluate the nanoparticles' antibacterial activity. Mueller-Hinton (MH) agar medium (15–20 mL) was added to sterilized petri plates to solidify. Following solidification, the test bacterial cell suspension (0.1%) was uniformly distributed across the agar surface using sterile cotton swabs. The sterile disc was filled with nanoparticles at several concentrations (25, 50, and 100 µg/mL) and had a diameter of 6 mm. Gentamicin (5 µg), a traditional antibiotic, was also added as a positive control to assess the nanoparticles' inhibitory effect. The disc was then positioned on the agar surface. Each plate was examined for a zone of inhibition following a 24-hour incubation period at 37 °C.The diameter of the growth inhibition was calculated by measuring the zone of inhibition.

3. Results and Discussion

3.1 UV DRS analysis

Fig. 1 (a-e) depicts the absorption behavior of TC1, TC2, TC3, TC4, and TC5 nanocomposites. Sharp absorbance peaks at 276–271 nm were seen in the figure. In comparison to other concentrations, TC3 (268 nm) has the highest absorbance and a blue-shifted absorbance, while TC5 (260 nm) has a lower absorbance and a red-shifted value (Table 1). This is because Ti-ion incorporation is significantly influenced by the $CaCO_3$/PMMA matrix [37]. The d-d transition of dopant ions from the ground state to an excited state appears to be responsible for the broad absorption band. Vacancies, impurity states, and structural alterations within the crystal lattice can result from this transition. These impurity states may result in defect energy levels and lattice deformation in the particles during preparation, which would reduce the band gap and increase absorption [38].

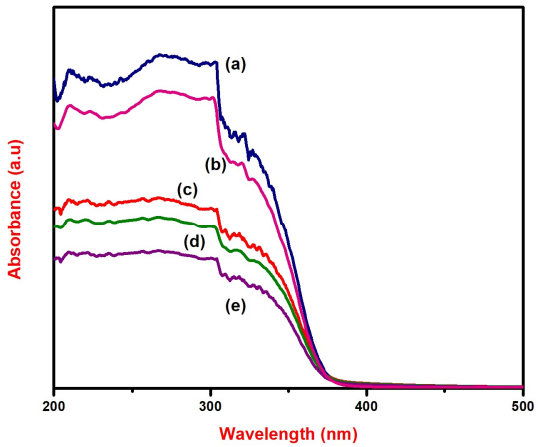

Fig. 1 UV-DRS spectra of (a) TC1, (b) TC2, (c) TC3, (d) TC4 and (d) TC5 nanocomposites

Table 1
Absorption and emission values of Ti doped $CaCO_3$/PMMA Nanocomposites

Samples	Absorption wavelength (nm)	PLE and PL analysis (nm)	
		Excitation	Emission
TC1	264	380	464
TC2	266	382	465
TC3	268	378	457
TC4	265		
TC5	260		

3.2 Photoluminescence

The PL spectra of TC1, TC3, and TC5 are displayed in Fig. 2 (a–c). These nanocomposites' excitation and emission wavelengths were evaluated based on the figure (Table 1). In comparison to the other products, the table indicates that TC5 (457 nm) has a blue-shifted emission value and TC3 (465 nm) has a red-shifted value. The same emission was noted by Gupta et al. [39], Saravanan et al. [40], and Kaur and Verma [41]. They came to the conclusion that either increased surface luminescence, vacancies, or oxygen surface traps were to blame. From the result, when the size shrank, the PL intensity rose dramatically. The TC3 and TC5 were selected for additional investigation based on the UV-DRS, and PL results.

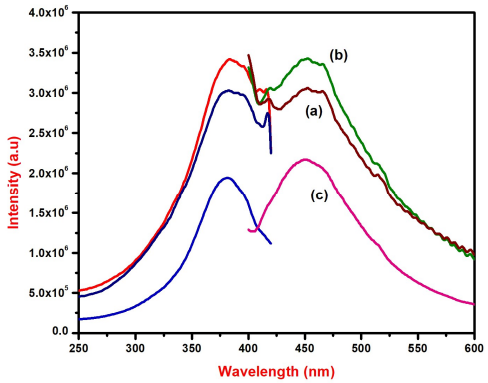

Fig. 2 PL spectra of (a) TC1, (b) TC3 and (c) TC5 nanocomposites

3.3 XRD

The XRD patterns of TC3 and TC5 are displayed in Fig. 3 (a–b). The obtained plane values (hkl) at coordinates 23.05◦, 29.41◦, 31.39◦, 35.92◦, 39.47◦, 43.12◦, 47.55◦, 48.52◦, 56.58◦, 57.37◦, 60.69◦, and 64.61◦ were noted from the figure Fig. 3 (a–b).

The rhombohedral structure and crystalline character of $CaCO_3$ in the calcite polymorph (JCPDS: 86–2342) are closely associated with these planes [36]. The absence of titanium metal or oxide phases in the figure indicates that Ti^{4+} has been incorporated into the host lattice [42].

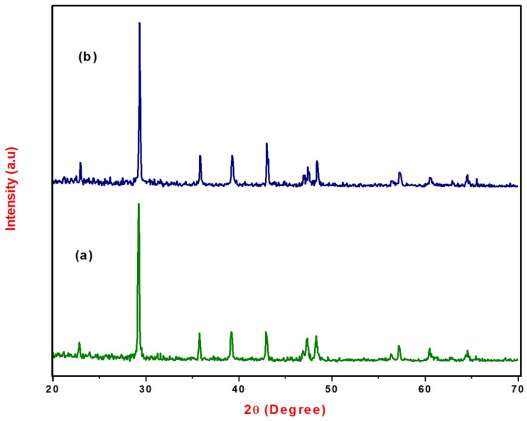

Fig. 4 XRD pattern of (a) TC3, and (b) TC5 nanocomposites

It shows the product in its unadulterated $CaCO_3$ state. Scherrer's formula was used to calculate the average crystallite sizes of TC3 and TC5 [43]. TC3 and TC5 had typical crystallite sizes of 35 and 25 nm, respectively. The formation energy of the nanocrystals is quite high, according to Venkidasamy et al. [35]. As a result, structural parameters including microstrain (□) and dislocation density (□) are computed. For TC3 and TC5, the microstrain values are $1.23x10^{-3}$ and $1.51x10^{-3}$, respectively, while the dislocation density values are $93.01x10^{12}$ and $113.76x10^{12}$.

3.4 FTIR

The FTIR spectra of TC3 and TC5 are shown in Fig. 4 and 5. Calcite-form carbonate peaks may be seen at approximately 712, 873, 1425, 1797, 2512, 2850, and 2930 cm^{-1} [43]. The presence of PMMA on the surface of $CaCO_3$ is shown by the absorption peaks at1091, 1084 cm^{-1} respectively [44].

Adsorbed OH stretching is responsible for the peaks at 3429–3427cm^{-1}[32]. The stretching vibration of Ti-O-Ti is responsible for the presence of peaks about 452 cm^{-1} [45].

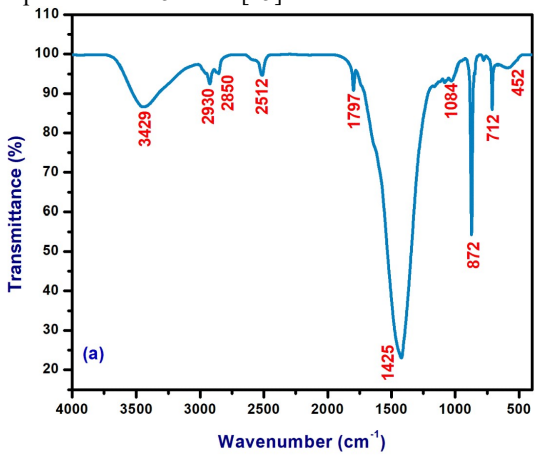

Fig. 4 FTIR spectra of TC3 nanocomposites

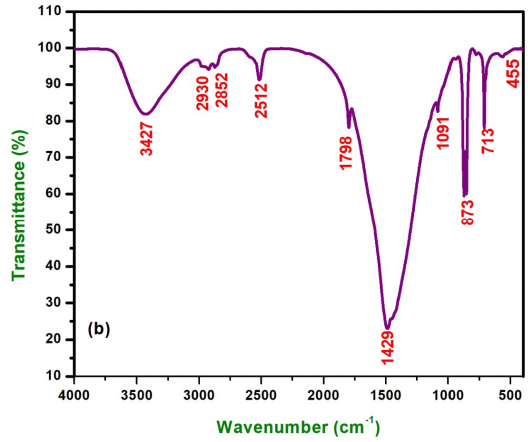

Fig. 5 FTIR spectra of TC5 nanocomposites

3.5 FESEM

The surface morphology of the TC3 and TC5 are shown in Fig. 5 (a-b). From these figure, the samples TC3 and TC5 has a rhombohedral form and is aggregated (Fig. 6 (a-b)).

Furthermore, the creation of complex aggregates through Ca binding to PMMA may encourage Ca^{2+} transport and aggregation, raising the calcium ion concentration [43].

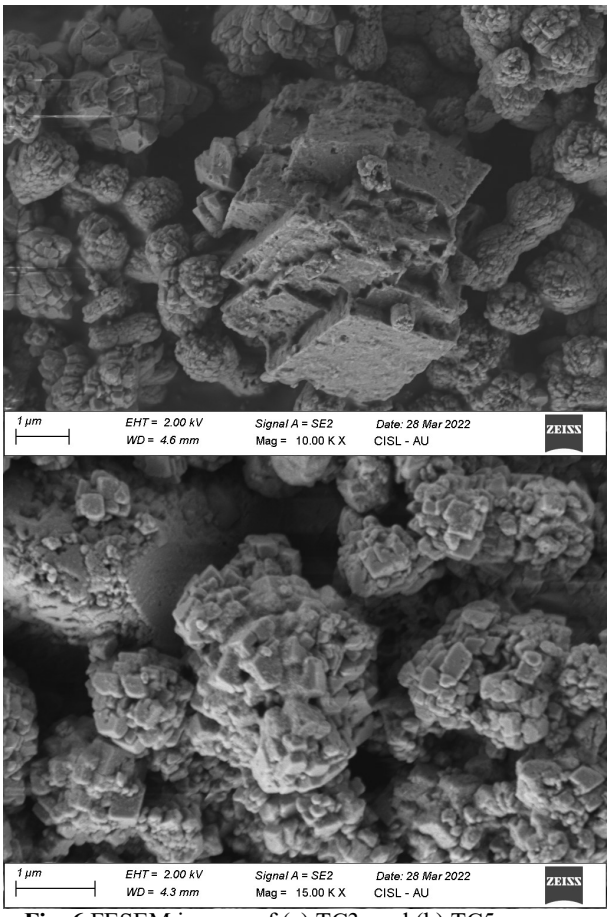

Fig. 6 FESEM images of (a) TC3, and (b) TC5 nanocomposites

3.6 Photocatalytic activity

Malachite green (MG) degradation under UV radiation employing TC3 photocatalysts. Figure 7 illustrates how the degradation performance was examined by measuring the absorbance of MG. The degradation of MG for TC3 photocatalysts was shown to decrease with the duration of UV irradiation (0 to 110 min).

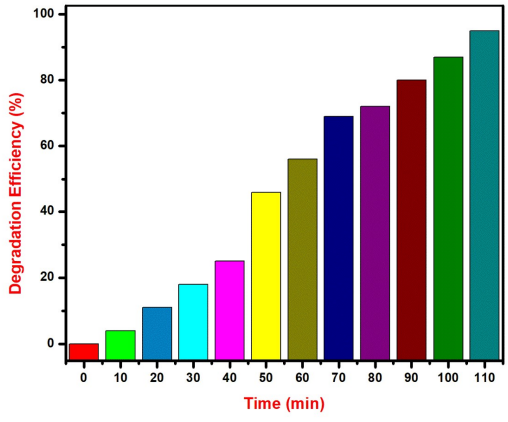

Fig. 7 Degradation efficiency of TC3 nanocomposites against Malachite green

This suggests that TC3 has improved photocatalytic activity to break down MG molecules over a 110-minute period. High surface areas are thought to facilitate interaction between surrounding molecules and electron-hole carriers [46, 47].

Pseudo-first-order kinetics [38] was used to estimate the degradation rate constant in the examination of MG degradation performance (Fig. 8). By following the curve's slopes, the degradation rate constant was determined. For TC3 photocatalysts, the MG degradation rate constant values were k = 0.0165 min^{-1}. The findings validate the effective photocatalytic activity of TC3 produced by burning for MG degradation [47]. Surprisingly, compared to previously published material [38], the degradation rate constant for TC3 photocatalysts rose by more than 95%.

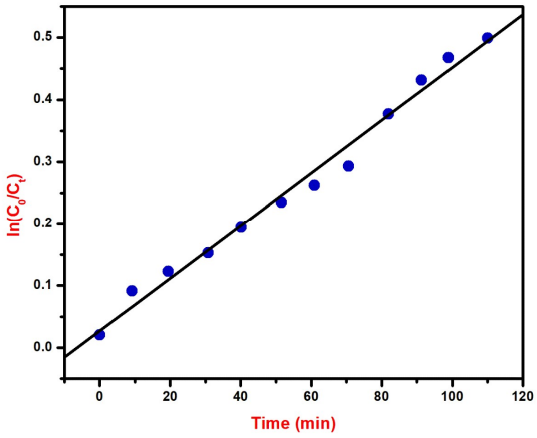

Fig. 8 Pseudo first order kinetics of TC3 nanocomposites

Below is a quick description of the photocatalytic degradation mechanism. As the photocatalyst is activated by absorbing photons, electron-hole (e^-/h^+) pairs are produced concurrently. Additionally, they constantly diffuse onto the surface of the photocatalyst [48].

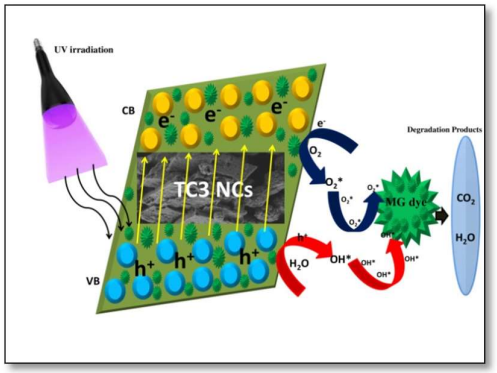

Fig. 9 Possible degradation mechanism of TC3 nanocomposites against MG dye

Superoxide radicals (O_2*) are produced when electrons in the MG solution react with dissolved oxygen (O_2). Hydroxyl radicals (OH*) are created when the holes react with water in a different process. MG dyes are effectively broken down into other compounds by these reactive radicals.

In this investigation, TC3 was used to monitor the MG solution both before and after the photocatalytic degradation for 110 minutes in order to analyze the products (Figure 9).

3.7 Antibacterial activity

Microorganisms and other contaminants are abundant in wastewater. In this case, TC5 plays a significant part in the antibacterial activity that removes and disinfects the effluent from living things. Table 2 displays the antibacterial test findings utilizing *S. aureus, S. pyogenes, K. pneumoniae, and E.coli* bacteria, whereas Fig. 10 displays an optical image of the inhibitory zone of the control, TC5 sample. The findings show that the composite heterojunction material sample have the largest inhibition zones for both gram positive and negative bacteria tests, while the control, gentamicin, has an inhibition zone of 29 mm.

This indicates that composite TC5 has created a new composite with greater antibacterial activity because the synthesized sample contains around 70% of the regulated gentamicin. The biocidal effect of the resulting inorganic antimicrobial substance against bacteria (*such as S. aureus, S. pyogenes, K. pneumoniae, and E.coli*) led to zone inhibition and bacterial death, which is one of its main advantages. Reactive oxygen species such hydroxyl radicals, superoxide, and H_2O_2 are produced when materials come into contact with the membrane of bacterial cells in the presence of moisture, which explains the antibacterial action mechanism [49].

The negatively charged particles found in OH* radicals and/or superoxide can damage proteins, lipids, and DNA by penetrating the cell membrane and remaining on the bacterial surface. In contrast, H_2O_2 acts as a disinfectant for the wastewater during the photocatalytic treatment process by penetrating the cell membrane and killing the bacteria [49].

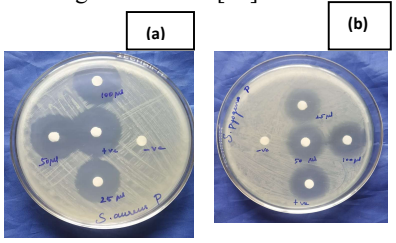

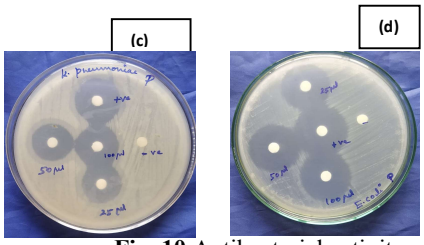

Fig. 10 Antibacterial activity of TC5 nanocomposites against (a) *S. aureus* (b) *S.pyogenes* (c) *K. pneumonia* and (d) *E. coli*. (250µg/mL, 500 µg/mL, 1000 µg/mL dose of TC5 nanocomposites and 5 µg/mL of Gentamicin – standard antibiotic)

4. Conclusion

In this work, a biomimetic method with different dopant concentrations was effectively used to prepare Ti-doped calcium carbonate nanocomposites (TC). The 0.06 M sample showed the best absorption and emission efficiency, and spectroscopic investigations verified that the optical characteristics of the nanocomposites are highly dependent on Ti content. Titanium was successfully incorporated into the $CaCO_3$ lattice while retaining its rhombohedral crystalline structure, with crystallite sizes in the nanorange (25–35 nm), according to structural and functional analysis using FTIR and XRD. The structure was primarily spherical, according to morphological examinations, and the presence of Ti ions in the host matrix was further verified by EDX analysis. The 0.06 M TC showed the best photocatalytic performance among the produced samples, degrading malachite green dye by up to 95% in 110 minutes when exposed to UV light. In the meantime, the 0.1 M TC demonstrated improved antibacterial activity against both Gram-positive and Gram-negative bacterial strains, suggesting that they are useful for biological applications at greater concentrations. Overall, the findings indicate that Ti-doped $CaCO_3$ nanocomposites have a great deal of promise as effective photocatalysts and antibacterial agents.

Conflict of Interest

The authors declare that there is no conflict of interest regarding the publication of this article.

Ethical approval and consent to participate

'Not applicable'

Availability of data and materials

The dataset generated and/or analyzed during the current study is available from the corresponding author upon reasonable request.

Author contribution

T. Sathishpriya: Methodology, Formal analysis, Data curation, and Visualization. **E.Thenpandiyan**: Conceptualization, methodology, Formal analysis, Data curation, Visualization, and original draft preparation. **D. Mohanambal**: Methodology, Reviewing, Formal analysis, Data curation, and Visualization. **Yengkokpam Robinson Singh:** Formal analysis, Data curation, and Visualization. **N. Prathap:** Methodology, Data curation, and Visualization. **A. Ajith:** Formal analysis, Reviewing and Editing

Reference

1. Mousa, H. M., Alenezi, J. F., Mohamed, I. M., Yasin, A. S., Hashem, A. F. M., & Abdal-Hay, A. (2021). Synthesis of TiO_2@ ZnO heterojunction for dye photodegradation and wastewater treatment. *Journal of Alloys and Compounds*, *886*, 161169.
2. Yudasari, N., Anugrahwidya, R., Tahir, D., Suliyanti, M. M., Herbani, Y., Imawan, C., ...& Djuhana, D. (2021). Enhanced photocatalytic degradation of rhodamine 6G (R6G) using ZnO–Ag nanoparticles synthesized by pulsed laser ablation in liquid (PLAL). *Journal of Alloys and Compounds*, *886*, 161291.
3. Arslan, I., & Balcioğlu, I. A. (1999). Degradation of commercial reactive dyestuffs by heterogenous and homogenous advanced oxidation processes: a comparative study. *Dyes and pigments*, *43*(2), 95-108.
4. Sahinkaya, E., Sahin, A., Yurtsever, A., & Kitis, M. (2018). Concentrate minimization and water recovery enhancement using pellet precipitator in a reverse osmosis process treating textile wastewater. *Journal of environmental management*, *222*, 420-427.
5. Bouazizi, A., Breida, M., Achiou, B., Ouammou, M., Calvo, J. I., Aaddane, A., & Younssi, S. A. (2017). Removal of dyes by a new nano–TiO2 ultrafiltration membrane deposited on low-cost support prepared from natural Moroccan bentonite. *Applied clay science*, *149*, 127-135. K.N. Aboua, Y.A. Yobouet, K.B. Yao, D.L. Goné, A. Trokourey, Investigation of dye adsorption onto activated carbon from the shells of Macoré fruit, *J. Environ. Manag.* 156 (2015) 10–14.
6. C. Galindo, P. Jacques, A. Kalt, Photooxidation of the phenylazonaphthol AO20 on TiO_2: Kinetic and mechanistic investigations, *Chemosphere* 45 (2001) 997–1005.
7. A. Gupta, N. Khosla, V. Govindasamy, A. Saini, K. Annapurna, S.R. Dhakate, Trimetallic composite nanofibers for antibacterial and photocatalytic dye degradation of mixed dye water, *Appl. Nanosci.* 10 (2020) 4191–4205.

8. G.P. Awasthi, S.P. Adhikari, S. Ko, H.J. Kim, C.H. Park, C.S. Kim, Facile synthesis of ZnO flowers modified graphene-like MoS_2 sheets for enhanced visible-light-driven photocatalytic activity and antibacterial properties, *J. Alloys Compd.* 682 (2016) 208–215.
9. S. Fang, K. Lv, Q. Li, H. Ye, D. Du, M. Li, Effect of acid on the photocatalytic degradation of rhodamine B over g-C_3N_4, *Appl. Surf. Sci.* 358 (2015) 336–342.
10. Z. Zhang, S. Zhai, M. Wang, H. Ji, L. He, C. Ye, C. Wang, S. Fang, H. Zhang, Photocatalytic degradation of rhodamine B by using a nanocomposite of cuprous oxide, three-dimensional reduced graphene oxide, and nanochitosan prepared via one-pot synthesis, *J. Alloys Compd.* 659 (2016) 101–111.
11. K. Kaviyarasu, A. Ayeshamariam, E. Manikandan, J. Kennedy, R. Ladchumananandasivam, U.U. Gomes, M. Jayachandran, M. Maaza, Solution processing of CuSe quantum dots: Photocatalytic activity under RhB for UV and visible-light solar irradiation, *Mater. Sci. Eng. B* 210 (2016) 1–9.
12. Ding, C.; Zhu, Q.; Yang, B.; Petropoulos, E.; Xue, L.; Feng, Y.; He, S.; Yang, L. Efficient photocatalysis of tetracycline hydrochloride (TC-HCl) from pharmaceutical wastewater using AgCl/ZnO/g-C_3N_4 composite under visible light: Process and mechanisms. J. Environ. Sci. 2023, 126, 249–262.
13. Lincho, J.; Zaleska-Medynska, A.; Martins, R.C.; Gomes, J. Nanostructured photocatalysts for the abatement of contaminants byphotocatalysis and photocatalytic ozonation: An overview. Sci. Total Environ. 2022, 837, 155776.
14. Liu, C.; Mao, S.; Shi, M.; Hong, X.; Wang, D.; Wang, F.; Xia, M.; Chen, Q. Enhanced photocatalytic degradation performance of $BiVO_4$/BiOBr through combining Fermi level alteration and oxygen defect engineering. Chem. Eng. J. 2022, 449, 137757.
15. Liu, C.; Mao, S.; Wang, H.; Wu, Y.; Wang, F.; Xia, M.; Chen, Q. Peroxymonosulfate-assisted for facilitating photocatalyticdegradation performance of 2D/2D WO_3/BiOBr S-scheme heterojunction. Chem. Eng. J. 2022, 430, 132806.
16. Liu, C.; Mao, S.; Shi, M.; Wang, F.; Xia, M.; Chen, Q.; Ju, X. Peroxymonosulfate activation through 2D/2D Z-scheme CoAl-LDH/BiOBr photocatalyst under visible light for ciprofloxacin degradation. J. Hazard. Mater. 2021, 420, 126613.
17. Qumar, U.; Hassan, J.Z.; Bhatti, R.A.; Raza, A.; Nazir, G.; Nabgan, W.; Ikram, M. Photocatalysis vs adsorption by metal oxide nanoparticles. J. Mater. Sci. Technol. 2022, 131, 122–166.
18. Cole, M.; Eggleston, G.; Wang, Y.J. Understanding the causes of calcium carbonate crystal growth and inhibition during the carbonatation refining of raw sugars. Food Chem. 2019, 275, 24–31.
19. Chong, K.Y.; Chia, C.H.; Zakaria, S.; Sajab, M.S. Vaterite calcium carbonate for the adsorption of Congo redfrom aqueous solutions. J. Environ. Chem. Eng. 2014, 2, 2156–2161.
20. Subramanian, M.N. Plastics Additives and Testing; John Wiley & Sons Inc.: Hoboken, NJ, USA, 2013.
21. Baláž, M.; Buj ˇnáková, Z.; Baláž, P.; Zorkovská, A.; Danková, Z.; Brianˇcin, J. Adsorption of cadmium(II) on waste biomaterial. J. Colloid Interface Sci. 2015, 454, 121–133.
22. Sayed, S.A.; El Sayed, A.S.; Zayed, A.M. Removal of oil spills from salt water by magnesium, calcium carbonates and oxides. J. Appl. Sci. Environ. Manag. 2005, 8, 71–78.
23. Zhao, D.H.; Gao, H.W. Turning calcium carbonate into a cost-effective wastewater-sorbing material byoccluding waste dye. Environ. Sci. Pollut. Res. 2010, 17, 97–105.
24. Sawhney, A.P.S.; Condon, B.; Singh, K.V.; Pang, S.S.; Li, G.; Hui, D. Modern Applications of nanotechnologyin textiles. Text. Res. J. 2008, 78, 731–739.
25. Yetisen, A.K.; Qu, H.; Manbachi, A.; Butt, H.; Dokmeci, M.R.; Hinestroza, J.P.; Skorobogatiy, M.; Khademhosseini, A.; Yun, S.H. Nanotechnology in textiles. ACS Nano 2016, 10, 3042–3068.
26. Mahltig, B.; Haufe, H.; Böttcher, H. Functionalisation of textiles by inorganic sol-gel coatings. J. Mater. Chem.2005, 15, 4385–4398.
27. Kashif, M., Jawad, M., Khan, A. A., Sun, H., Ullah, K., Fakayode, O., &Azizi, S. (2024). Fe/Ti-codoped strontium oxide nanoparticles for enhanced photocatalytic degradation of methyl orange. *Journal of Applied Research in Water and Wastewater*, *11*(1), 8-14.
28. Das A, Chowdhury BN, Saha R, Sikdar S, Bhunia S, Chattopadhyay S. Ultrathin

Vapor–Liquid–Solid Grown Titanium Dioxide-II Film on Bulk GaAs Substrates for Advanced Metal–Oxide–Semiconductor Device Applications. IEEE Trans on Elect Dev 2018;65(4):1466–72.
29. Safajou H, Khojasteh H, Salavati-Niasari M, Mortazavi-Derazkola S. Enhanced photocatalytic degradation of dyes over graphene/Pd/TiO_2 nanocomposites:TiO_2 nanowires versus TiO_2 nanoparticles. J of coll and interfsci 2017;498:423–32.
30. Low FW, Lai CW. Recent developments of graphene-TiO_2composite nanomaterials as efficient photoelectrodesindye-sensitized solar cells: a review. Renew and Sustain EnerRev 2018;82:103–25.
31. Stoyanova A, Hitkova H, Bachvarova-Nedelcheva A, Iordanova R, Ivanova N, Sredkova M. Synthesis and antibacterial activity of TiO_2/ZnO nanocomposites prepared via non hydrolytic route. J Chem Technol Metall 2013;48(2):154–61
32. Wang Y, Xue X, Yang H. Modification of the antibacterial activity of Zn/TiO_2 nano-materials through different anionsdoped. Vacuum 2014; 101:193–9.
33. Kaviyarasu K, Geetha N, Kanimozhi K, Magdalane CM, Sivaranjani S, Ayeshamariam A, et al. In vitro cytotoxicity effect and antibacterial performance of human lungepithelial cells A549 activity of zinc oxide doped TiO_2 nanocrystals: investigation of bio-medical application bychemical method. Mater Sci Eng C 2017; 74:325–33.
34. Venkidasamy, R., Elumalai, T., Govindhasamy, S., Tharmalingam, S., & Emmanuel Rajan, J. J. S. (2024). Synthesis of $CaCO_3$ nanocomposite from natural carbonate source and its effect on the inclusion of Eu^{3+} ions for photocatalytic activity. *Chemical Engineering Communications*, *211*(2), 229-250.
35. D. Zhang, Structural, optical, electrical, and photocatalytic properties of manganese-doped zinc oxide nanocrystals, *Russ. J. Phys. Chem. A* 86 (2012) 93–99.
36. Sathishpriya, T., Thenpandiyan, E., Suresh, G., Ramasamy, V., Kumar, S. R. A., & Senthil, S. (2025). Impact of Mg-doped $CaCO_3$/PMMA nanocomposites on their performance of photocatalytic and antibacterial activities. *Chemical Physics Impact*, 100968.
37. M. Kaur, N.K. Verma, $CaCO_3$/TiO_2 nanoparticles-based dye-sensitized solar cell, *J. Mater. Sci. Technol.* 30 (2014) 328–334.
38. L. Saravanan, S. Diwakar, R. Mohankumar, A. Pandurangan, R. Jayavel, Synthesis, structural and optical properties of PVP-encapsulated CdS nanoparticles, *Nanomater. Nanotechnol.* 1 (2011) 17.
39. U. Gupta, V.K. Singh, V. Kumar, Y. Khajuria, Experimental and theoretical spectroscopic studies of calcium carbonate ($CaCO_3$), *Mater. Focus* 4 (2015) 164–169.
40. Mozammel, M., NajibiIlkhechi, N., Ghezelbash, B., &Nasiri Khalil Abad, S. (2019). Antibacterial and heavy ion removal properties of La-and Ti-doped ZnO nanoparticles. *Materials Research Express*, *6*(8), 085010.
41. Ramasamy, V., Sathishpriya, T., Thenpandiyan, E., & Suresh, G. (2023). Fabrication of eco-friendly UV-visible driven Ni: $CaCO_3$ photocatalyst for sustainable environmental remediation. *Asian Journal of Chemistry*, *35*(3), 692-704.
42. Pal, M. K., Singh, B., & Gautam, J. (2012). Thermal stability and UV-shielding properties of polymethyl methacrylate and polystyrene modified with calcium carbonate nanoparticles. *Journal of thermal analysis and calorimetry*, *107*(1), 85-96.
43. Pragathiswaran, C., Smitha, C., Abbubakkar, B. M., Govindhan, P., & Krishnan, N. A. (2021). Synthesis and characterization of TiO_2/ZnO–Ag nanocomposite for photocatalytic degradation of dyes and anti-microbial activity. *Materials Today: Proceedings*, *45*, 3357-3364.
44. Sujinnapram, S.; Wongrerkdee, S. Synergistic effects of structural, crystalline, and chemical defects on the photocatalytic performance of Y-doped ZnO for carbaryl degradation. J. Environ. Sci. 2023, 124, 667–677.
45. Siva, N.; Kannadasan, N.; Shanmugam, N.; Ragupathy, S.; Sakthi, D.; Arun, V. Effect of Ti-doping on photocatalytic activity of ZnO nanocatalyst under sunlight irradiation. Inorg. Chem. Commun. 2022, 146, 110097.

46. Buasakun, J.; Srilaoong, P.; Chaloeipote, G.; Rattanakram, R.;Wongchoosuk, C.; Duangthongyou, T. Synergistic effect of ZnO/ZIF8 heterostructure material in photodegradation of methylene blue and volatile organic compounds with sensor operating at room temperature. J. Solid State Chem. 2020, 289, 121494
47. Zhou, Y., Tan, Y., Xiang, Y., & Zhu, J. (2019). Construction of urchin-like ZnO/TiO2 direct Z-scheme system to improve charge separation. *ChemistrySelect*, *4*(44), 12963-12970.
48. Tankhiwale, R., & Bajpai, S. K. (2012). Preparation, characterization and antibacterial applications of ZnO-nanoparticles coated polyethylene films for food packaging. *Colloids and surfaces B: Biointerfaces*, *90*, 16-20.